ACS OMEGA

Open Access

http://pubs.acs.org/journal/acsodf

Article

Process Condition Optimization and Structural Feature Analysis of Humic Acid Extraction from Weathered Lignite

Yan Yang, Yanhong Li,* Yuanqin Zhang, Miao Wang, Pingyan Wang, and Donghui Liu

Cite This: *ACS Omega* 2024, 9, 38409−38422

Read Online

ACCESS | Metrics & More | Article Recommendations | Supporting Information

ABSTRACT: In this study, response surface methodology (RSM) was adopted to investigate the optimization of process conditions for extracting humic acid (HA) from coal, aiming to enhance the yield of humic acid. Additionally, UV−vis spectroscopy, FTIR, XRD, TG-DTG, CP/MAS^{13}CNMR, XPS, and molecular fluorescence were utilized to examine the properties of HAs. The extraction time significantly influenced the yield from Lishi weathered lignite, while the liquid−solid ratio had a significant impact on the yield from Wuhai weathered lignite. The interactive effect between factors did not have a significant effect on the yield. The optimal extraction conditions for Lishi humic acid (LSHA) were determined to be an extraction time of 4.4 h, NaOH concentration of 0.30 mol/L, and liquid−solid ratio of 21 mL/g, while those for Wuhai humic acid (WHHA) were 3.1 h, 0.21 mol/L, and 12 mL/g, respectively. Under these optimal conditions, the true yield values closely matched the predicted value obtained from the model optimization. Comparative analysis of the HAs revealed similarities in their chemical properties, including the degree of aromaticity, molecular weight, and distribution of functional groups. The aromaticity of WHHA was higher compared to that of LSHA. The higher hydrophilic−hydrophobic index of LSHA contributed to its relatively high biological activity compared to that of WHHA. Both humic acids belong to terrestrial humic acids. The results of the study provide a reference for further application of humic acid.

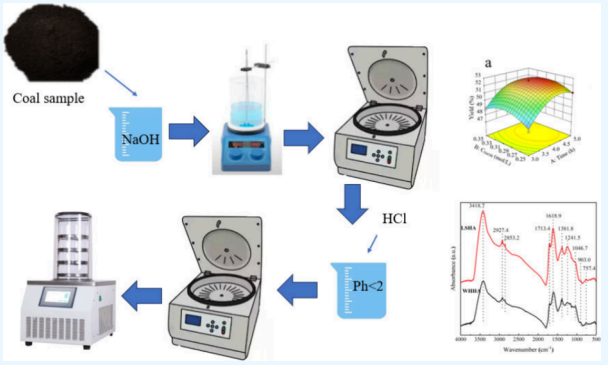

1. INTRODUCTION

Humic acid (HA) is a mixture of macromolecular organic compounds naturally formed through the decomposition and transformation of plants by microorganisms, followed by long-term geochemical processes.[1] This compound possesses numerous reactive functional groups, such as carboxyl and phenolic hydroxyl groups, which possess excellent physiological activity and functions including absorption, complexation, and ion exchange.[2,3] Additionally, these unique characteristics facilitate its widespread applications in agriculture, environmental protection, medicine, and industry.[4−7] Low-grade coals, such as peat, lignite, and weathered coal, have low utilization value as fuels and are currently the main raw materials for the production of humic acid. Weathered lignite typically contains 30−80% humic acid, with the specific content depending on the original characteristics of the coal and the conditions of the weathering process.[8] However, the extraction of HA from natural sources, particularly from coal, presents challenges due to low extraction rates, high energy consumption, and limited economic benefits. Therefore, it is crucial to optimize the extraction process of this compound to ensure the maximum yield and purity. Additionally, further exploration and enhancement of its potential applications in various fields are essential to harness its full potential.

In this context, response surface methodology (RSM) offers a promising approach for modeling and optimizing the extraction process. The RSM provides a systematic framework for studying the interaction between multiple factors and optimizing the extraction conditions, thus minimizing the number of experimental runs and enhancing the efficiency of the process.[9,10] Ehsan Sarlaki et al. employed a three-level, three-factor central composite design to model and optimize the extraction process of humic acid from lignite waste, achieving the highest extraction efficiency of 54.2% for HA during their study.[11]

Currently, the alkali-dissolution and acid-precipitation methods are primarily used to extract humic acid from organic substances such as coal. This method leverages the fact that humic acid is soluble in alkali but insoluble in acid. The humic acid is initially dissolved in a NaOH/KOH solution and then precipitated out using a HCl solution.[11−14] This study is based

Received: February 25, 2024
Revised: July 12, 2024
Accepted: August 14, 2024
Published: September 3, 2024

on an alkaline extraction method and aims to apply RSM to investigate the extraction of HA from weathered lignite in Inner Mongolia Wuhai (WH) and Shanxi Lishi (LS), with a focus on understanding the influence of various factors on the yield of HAs and optimizing the extraction conditions. The composition and properties of extracted HA were thoroughly analyzed. Comprehensive characterization techniques including elemental analysis, UV−vis spectroscopy, FTIR, XRD, TG-DTG, CP/MAS^{13}CNMR, XPS, and molecular fluorescence were employed for this purpose. This study will provide valuable insights into the industrial production and further application of HA.

2. EXPERIMENTAL SECTION

2.1. Materials. Coal samples were acquired from leonardite in Wuhai (WH) of Inner Mongolia and Lishi (LS) of Shanxi Province, China. The raw coal samples were finely milled to a grain size of less than 0.2 mm. Sodium hydroxide (NaOH) was purchased from Tianjin Fengchuan Chemical Reagent Co., Ltd., and hydrochloric acid (HCl, 37%) was purchased from Chongqing Chuandong Chemical (Group) Co., Ltd. All reagents used were of analytical grade.

2.2. Total Humic Acid in Coal. The total humic acid content in the raw coal was determined by the volumetric method.[15] A sodium pyrophosphate alkaline solution was used to extract humic acid from the coal sample, and then, the carbon in humic acid was oxidized to carbon dioxide by potassium dichromate in a strongly acidic solution. The content of humic acid in the raw coal sample was calculated based on the consumption of potassium dichromate and the carbon content of humic acid.

2.3. HA Extraction from the Coal Sample. In this study, humic acids were extracted from coal using the alkali-dissolution and acid-precipitation method. The coal samples and NaOH solution were added into a conical flask at a certain liquid−solid ratio (the ratio of alkaline solution volume to coal sample mass, mL/g). The conical flask was reacted for a variable time, ranging from 1 to 6 h at room temperature (298 K, taking into account the issue of production costs in the actual industrial production process). After centrifugation (7000 rpm, 5 min) and suction filtration, the pH of the sample was modulated to less than 2 by HCl and left to stand for 24 h. The precipitate of HA was separated by centrifugation and then dialyzed. Finally, the HA sample was dried by using a freeze-dryer.

2.4. RSM Optimization Experiment. Based on the single-factor experimental results, the effects of the time, NaOH solution concentration, and liquid−solid ratio on extraction efficiency of HA (%) were investigated using a Box−Behnk design. Design-Expert was for developing three-factor and three-level experiments. A total of 17 test points, 12 analysis points, and 5 zeros were designed to assess the error (Table 1 and Table 2). Three coded ranges—low (−1), center (0), and high (1)—were nominated from the subsequent preliminary experimentation (Table S1). To assess the significance of each regression coefficient on HA extraction efficiency, an analysis of variance (ANOVA) was carried out. The optimum conditions to simulate the humic acid extraction process were used as the response surface model. A quadratic equation (eq 1) was employed for the approximation of resulting HA percentage extraction.

Table 1. RSM-BBD Design and Results of LSHA[a]

	LSHA				
	Factor			HA Extraction (%)	
No.	A	B	C	Actual Value	Predictive Value
1	4	0.30	20	51.9	52.3
2	5	0.25	20	50.9	50.9
3	3	0.30	16	48.2	47.9
4	4	0.25	16	49.7	49.6
5	5	0.30	24	51.1	51.3
6	4	0.25	24	50.9	50.7
7	4	0.30	20	52.7	52.3
8	4	0.30	20	52.2	52.3
9	5	0.30	16	50.7	50.8
10	4	0.35	16	49.9	50.1
11	4	0.35	24	50.5	50.6
12	4	0.30	20	52.3	52.3
13	5	0.35	20	51.1	50.8
14	3	0.30	24	49.1	48.9
15	3	0.25	20	47.7	47.9
16	3	0.35	20	48.4	48.4
17	4	0.30	20	52.7	52.3

[a]A is the time, h; B is the NaOH solution concentration, mol/L; C is the liquid−solid ratio, mL/g.

Table 2. RSM-BBD Design and Results of WHHA[a]

	WHHA				
	Factor			HA Extraction (%)	
No.	A	B	C	Actual Value	Predictive value
1	3	0.25	5	60.8	60.4
2	3	0.20	10	69.4	68.9
3	2	0.20	15	63.0	63.5
4	3	0.25	15	67.3	66.8
5	4	0.15	10	64.1	63.9
6	3	0.20	10	68.5	68.9
7	4	0.20	15	65.1	64.8
8	4	0.25	10	64.1	64.9
9	3	0.20	10	69.3	68.9
10	2	0.25	10	62.9	63.0
11	3	0.15	5	56.9	57.5
12	3	0.15	15	65.2	65.5
13	3	0.20	10	68.7	68.9
14	4	0.20	5	59.8	59.3
15	3	0.20	10	68.9	68.9
16	2	0.20	5	54.3	54.6
17	2	0.15	10	60.7	59.9

[a]A is the time, h; B is the NaOH solution concentration, mol/L; C is the liquid−solid ratio, mL/g.

$$Y = d_o + \sum_{i=1}^{k} d_i X_i + \sum_{i=1}^{k} d_{ii} X_i^2 + \sum_{i=1}^{k} \sum_{j=i+1}^{k} d_{ij} X_i X_j \quad (1)$$

where Y is response variable (HA extraction efficiency), d_0 is the intercept value, d_i (i = 1, 2, ..., n) is the first-order model coefficients for X_i, d_{ij} is the interaction coefficients for X_iX_j, and d_{ii} represents the quadratic coefficients of X_i.

2.5. Chemical and Spectral Features Analysis. The proximate analysis was subjected to testing with reference to GB/T 212-2008.[16] The moisture content was measured by air drying in a blast drying oven. The ash and volatile yields of the samples were automatically determined by an intelligent muffle

https://doi.org/10.1021/acsomega.4c01840
ACS Omega 2024, 9, 38409−38422

Table 3. ANOVA Analysis of Response Surface Model

	LSHA						WHHA					
Source	Sum of Squares	DfES	Mean Square	*F* value	*P* value	Remark	Sum of Squares	def.	Mean Square	*F* value	*P* value	Remark
Model	38.16	9	4.24	30.64	<0.0001	[c]	317.68	9	35.30	71.49	<0.0001	[c]
A	13.47	1	13.47	97.32	<0.0001	[c]	18.24	1	18.24	36.94	0.0005	[c]
B	0.063	1	0.063	0.46	0.5215	[a]	8.43	1	8.43	17.06	0.0044	[c]
C	1.21	1	1.21	8.74	0.0212	[b]	103.18	1	103.18	208.97	<0.0001	[c]
AB	0.078	1	0.078	0.57	0.4762	[a]	1.12	1	1.12	2.28	0.1752	[a]
AC	0.058	1	0.058	0.42	0.5394	[a]	2.89	1	2.89	5.85	0.0461	[b]
BC	0.099	1	0.099	0.72	0.4251	[a]	0.68	1	0.68	1.38	0.2788	[a]
A^2	11.42	1	11.42	82.51	<0.0001	[c]	67.16	1	67.16	136.02	<0.0001	[c]
B^2	5.86	1	5.86	42.31	0.0003	[c]	17.03	1	17.03	34.50	0.0006	[c]
C^2	3.64	1	3.64	26.27	0.0014	[c]	81.75	1	81.75	165.57	<0.0001	[c]
Residual	0.97	7	0.14				3.46	7	0.49			
Lack of fit	0.45	3	0.15	1.14	0.4339	[a]	2.85	3	0.95	6.27	0.0524	[a]
Total	39.13	16					321.14	16				

[a]Not significant ($P > 0.05$). [b]Significant ($P < 0.05$). [c]Extremely significant ($P < 0.01$).

furnace with model 5E-MF6100K (Changsha Kaiyuan Instrument Co., Ltd.), and the fixed carbon content could be obtained by using the subtraction method. The elemental compositions (C, H, N, and S) were determined with an elemental analyzer of the Vario macro cube model produced by Elementary, Germany. Oxygen content was calculated by the difference.

The contents of total acid groups and carboxyl groups were determined by the barium ion and calcium ion exchange methods, respectively.[17] The phenolic hydroxyl groups were determined by the difference between the total acid groups and the carboxyl groups. Ultraviolet−visible spectroscopy (UV−vis) analysis was carried out by a UV-1800PC Series (Shanghai Mepoda Instrument Co., Ltd.). For absorbance measurements, the humic acids were dissolved in 100 mL of $NaHCO_3$ solution (0.05 mol/L), and the absorbance (Abs) was measured at 400, 465, 600, and 665 nm. The E4/E6 ratios (Abs_{465}/Abs_{665}) and ΔLog *K* coefficients (Log Abs_{400} − Log Abs_{600}) were calculated for characterization of HAs.[18]

FT-IR spectra were recorded on a Fourier transform infrared spectrometer (model Nicolet iS50) using the KBr pellet technique. The spectrum was recorded from 4000 to 500 cm^{-1} at a resolution of 4 cm^{-1}. The thermal analyses (TG-DTG) of the HA samples were carried out in a thermal analyzer (model Netzsch STA 449F3) in an air atmosphere. A heating rate of 10 °C/min was chosen based on previous studies with continuous heating from 25 to 900 °C. Solid-state CP/MAS ^{13}C NMR spectra of the HAs were collected on an AVWBIII600 nuclear magnetic resonance spectroscopy instrument produced by Bruker. The test speed was 14 kHz, and the resonance frequency was 150.9 MHz.

The X-ray diffraction (XRD) spectra were obtained with an X-ray diffractometer (X'Pert 3, Panalytical, Netherlands). Samples were scanned over a 2θ range from 5 to 90 with a scanning voltage of 40 kV and target Cu/Kα (λ = 1.5406 Å).[18] XPS spectra were measured with a PHI5000 Versaprobe-II spectrometer (50 W, 15 kV). The Al target was selected as the X-ray light source. High-resolution spectra were obtained using 46.95 eV pass energy, and the spectra were corrected by C 1s with the binding energy of 284.8 eV. All fluorescence spectra were run on a Hitachi F-4600 fluorophotometer with a scan speed of 120 nm/min^{-1}, using excitation and emission slit bandwidths of 5 mm. Xe was used as the measuring light source. The scanning speed for three-dimensional fluorescence determination was 12 000 nm/min.

3. RESULTS AND DISCUSSION

3.1. Optimization of HA Extraction Conditions. The initial experimental results are shown in Figure S1. For LSHA, as the extraction time increases from 2 h to 5 h, the yield shows an upward trend, rising from 32.12% to 40.96%; for WHHA, as the extraction time increases from 1 h to 5 h, the yield shows an upward trend, rising from 62.57% to 66.53% (Figure S1(1,4)). However, with the prolongation of extraction time, both the extraction amounts of LSHA and WHHA decrease. This phenomenon can be attributed to the ease of decomposition and degradation of HA under extended extraction conditions.[19,20] Longer time periods correspond to increased energy usage and financial consequences. Thus, a time range of 3−5 h was chosen for additional optimization studies on LSHA extraction and 2−4 h for additional optimization on WHHA extraction. Once the optimal extraction time had been determined, HA extraction was studied using various NaOH concentrations. Figure S1(2,5) depicts that HA extraction increased significantly with an increase in NaOH concentration (LSHA: 0.15−0.30 mol/L; WHHA: 0.1−0.2 mol/L). Then, when the concentration of NaOH exceeds 0.3 mol/L for LSHA and 0.2 mol/L for WHHA, respectively, the extraction rates of both HA types decrease. Considering these data, NaOH concentrations in the range of 0.25−0.35 and 0.15−0.25 mol/L were carefully chosen for further optimization studies. This could prevent the need for using excessive solvent during the HA extraction process. The liquid−solid ratio presented the same trend as extraction time and NaOH concentration in extraction of two HAs.[21] Within the ranges of 10 to 20 for LSHA and 5 to 10 mL/g for WHHA, respectively, the yields of LSHA and WHHA increase as the liquid−solid ratio increases. Beyond these ranges, the yields of HAs gradually decrease. Based on the current experiment, the liquid−solid ratio in the range of 16−24 mL/g for LSHA and 5−15 mL/g for WHHA was chosen for additional optimization studies (Figure S1(3,6)).

After conducting initial screening experiments, the matrix design for the trials is presented in Table 1 and Table 2, using the Box−Behnken design. The analysis reveals a small deviation between the actual values of the two HAs of yields and the predicted values of the model. By comparing the fitting

https://doi.org/10.1021/acsomega.4c01840
ACS Omega 2024, 9, 38409−38422

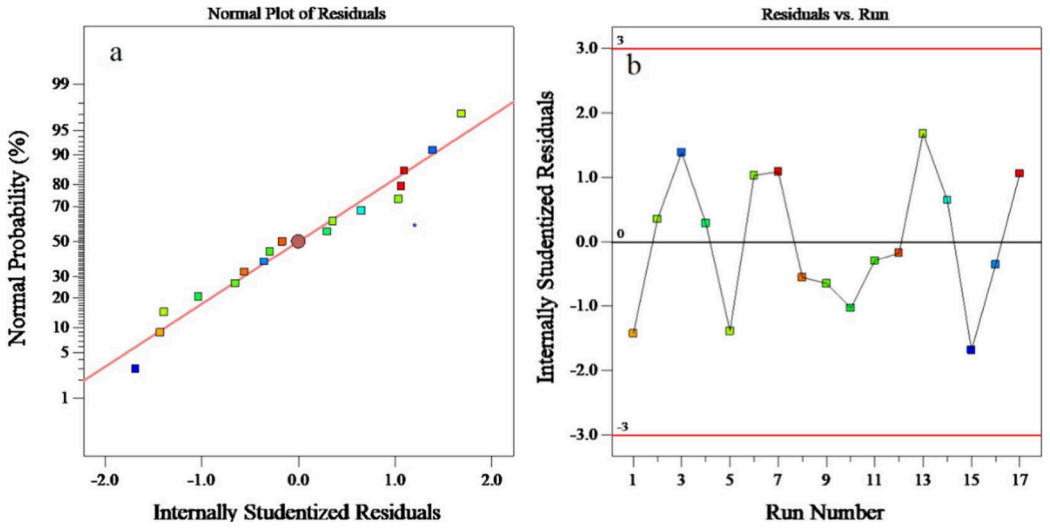

Figure 1. (a) Normal plot of residuals and (b) residuals of LSHA yield.

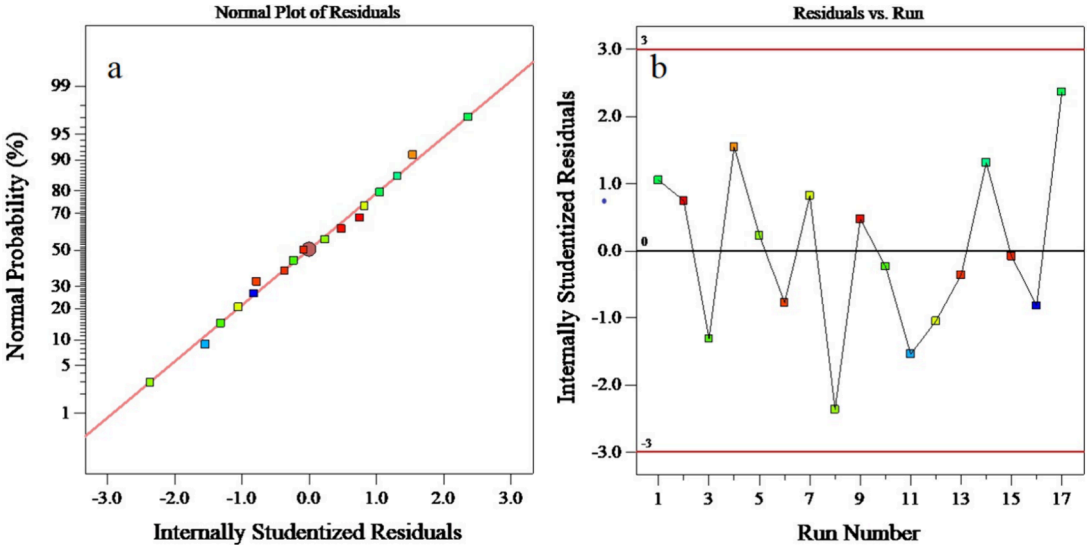

Figure 2. (a) Normal plot of residuals and (b) residuals of the WHHA yield.

degrees of the various fitting equations, two quadratic multiple regression equations have been derived:

$$Y_{LSHA} = -57.85 + 15.91A + 311.75B + 2.78C - 2.80AB - 0.03AC - 0.79BC - 1.65A^2 - 471.70B^2 - 0.06C^2 (R^2 = 0.9752;\ R^2_{adj} = 0.9434) \quad (2)$$

$$Y_{WHHA} = -47.36 + 29.29A + 390.63B + 5.09C - 10.60AB - 0.17AC - 1.65BC - 3.99A^2 - 804.50B^2 - 0.18C^2 (R^2 = 0.9892;\ R^2_{adj} = 0.97540) \quad (3)$$

Table 3 depicts the results of the analysis of variance, which showed that the *P*-values of the two models were both less than 0.0001, indicating that both models were significant. The *P*-value of the lack-of-fit was relatively low ($P > 0.05$), indicating that the lack-of-fit was not significant. This indicates that two models have a good fitting degree within the respective regression range, comply with the experimental requirement, and could be used for statistical analysis on experimental results.[22] The correlation coefficient (R^2) and adjusted correlation coefficient (R^2_{adj}) were both higher than 0.90. The experimental results showed that the model was in good agreement with the predicted results, and the experimental error was low, which can describe the relationship between the factors and their response values well. According to the experimental data, the residual probability distribution diagram and the residual curve of yields are drawn as shown in Figure 1 and Figure 2. The residual distribution was on both sides of the prediction curve, and there was no systematical bias toward over- or underestimating humic acid yields. Therefore, the error could be considered to follow the normal distribution, and the residual curve of yields further verifies the assumption that the error follows this distribution. Based on this analysis, the results have shown that the two models can effectively predict and analyze the extraction process of humic acid from both types of weathered lignite. The statistical significance, excellent fit, high correlation coefficients, low experimental error, and normal distribution of errors all indicate that the two models are highly effective tools for understanding and optimizing the extraction of humic acid from weathered lignite. In practical terms, these results

https://doi.org/10.1021/acsomega.4c01840
ACS Omega 2024, 9, 38409−38422

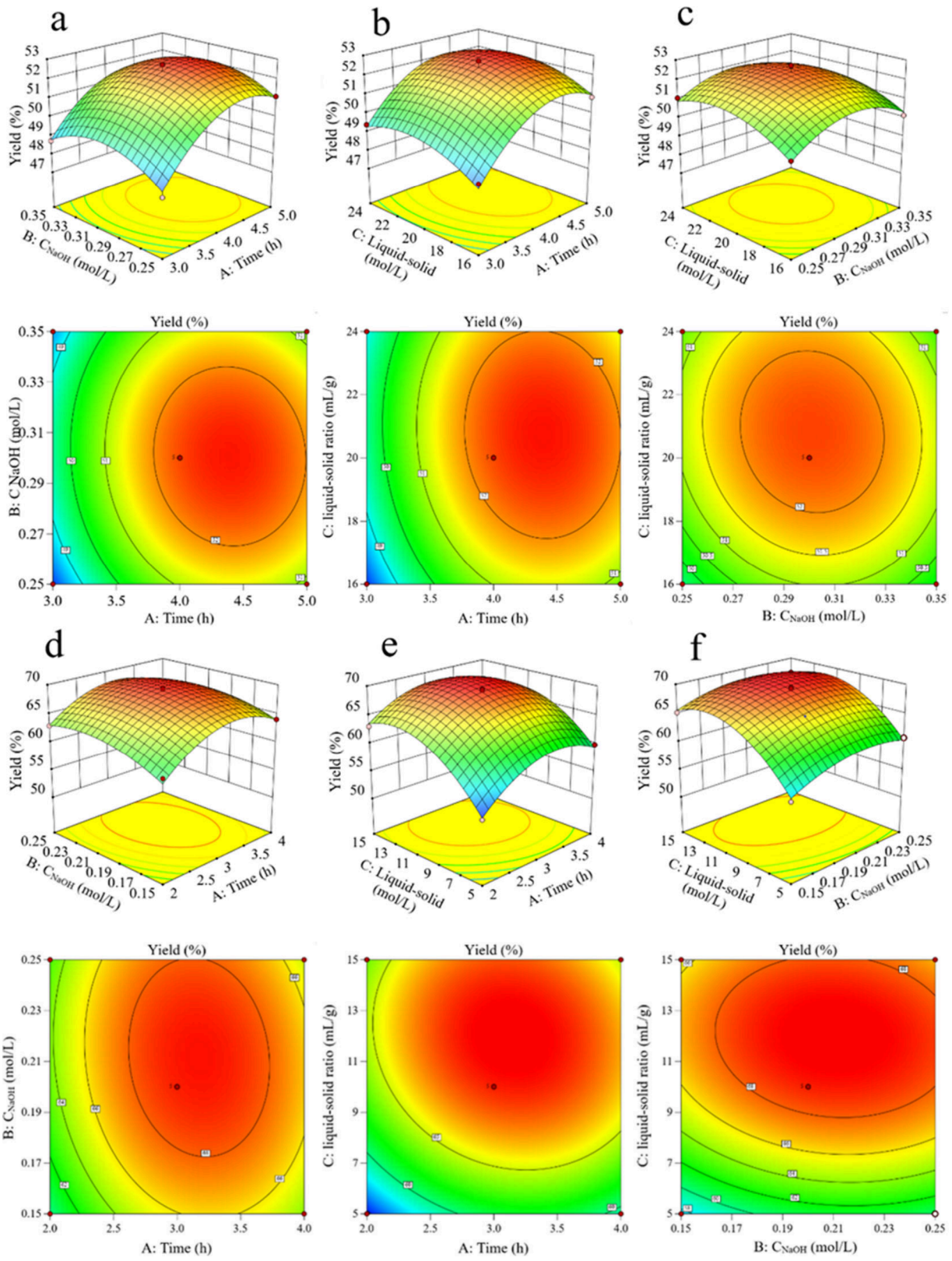

Figure 3. Contour and response surface plots showing the effect of interaction between two factors on HA yield (LSHA: a, b, c; WHHA: d, e, f).

mean that researchers can use the RSM to establish models to predict optimal extraction conditions for maximizing the humic acid yield from weathered lignite.

Figure 3 reflects the impact of the interaction between AB, AC, and BC on the yields of HAs in Table 3. The 3D response surface can reflect the influence of various factors on the response value of the model. The contour diagram is the projection of three-dimensional graphics. The yield of HA increased and decreased with the increase of extraction time (A), sodium hydroxide solution concentration (B), and

https://doi.org/10.1021/acsomega.4c01840
ACS Omega 2024, 9, 38409−38422

Table 4. Proximate Analyses and HA Yield[a]

Sample	Yield (%)	Proximate analyses (%)				Ultimate analyses (%, daf)				
		M_{ad}	A_d	V_{daf}	FC_{daf}	C	H	N	S	O
WH	-	3.6	54.62	45.5	54.5	62.41	4.55	1.21	4.55	27.27
LS	-	7.79	44.37	51.8	48.2	64.29	3.41	1.46	1.6	29.24
WHHA	52.77	8.74	4.12	-	-	62.83	4.19	1.32	0.15	31.51
LSHA	69.52	10.64	5.09	-	-	59.04	4.25	1.34	0.22	35.15

[a]A_d is air-dried basis; d is dry basis; daf is dry ash free basis.

liquid−solid ratio (C). As shown in Figure 3(a, b, c), in the process of extracting HA from weathered lignite in Lishi, the results indicate that A exerts a paramount influence on HA yield, corroborating its pivotal role in facilitating the release of HAs from the lignite matrix. Meanwhile, C demonstrates a moderately significant impact, suggesting that optimizing this parameter can further enhance the yield. Conversely, B and the interaction terms AB, AC, and BC had a certain but not significant impact, implying that the studied range adjustments to this parameter may not yield substantial gains in HA yield. As described in Figure 3(d, e, f), in the process of extracting HA from weathered lignite in Wuhai, C emerges as the most critical factor, emphasizing the importance of solvent quantity in enhancing mass transfer and, consequently, HA dissolution. Additionally, A, B, and interaction item AC significantly contribute to yield, indicating that a synergistic adjustment of these parameters is crucial for maximizing HA recovery. Notably, interaction items AB and BC are found to be insignificant, suggesting that their combined effect does not significantly alter the overall yield trend. The analysis results of the *F* value and *P* value in Table 3 were consistent with this. The significant differences between Lishi and Wuhai in the process of HA extraction indicate that geographical factors have a crucial impact on the extraction efficiency. This may be attributed to the disparities in physicochemical properties such as mineral composition, organic matter content, and particle size distribution of the weathered lignite in the two regions. In summary, the extraction efficiency of humic acid is jointly influenced by various factors, including extraction time, sodium hydroxide solution concentration, and liquid-to-solid ratio, as well as the interactions among these factors. Furthermore, regional differences also constitute a significant factor that cannot be overlooked. To enhance the extraction efficiency of HA, it is recommended to implement customized production based on raw materials sourced from different regions. This can be achieved by optimizing the extraction conditions, particularly the extraction time and liquid-to-solid ratio, and taking into account the interactions among factors to realize efficient extraction.

3.2. Determination and Verification of Optimum Process Conditions. The optimization function of Design-Expert10.4.4 software was used to optimize the extraction conditions of LSHA and WHHA with 100% HA yield as the target value. Optimal extraction conditions of LSHA were as follows: the extraction time was 4.4 h, the NaOH concentration was 0.30 mol/L, the liquid/solid ratio was 20.74 mL/g, and the maximum yield of LSHA predicted by the model was 52.8%. Integer values for the liquid−solid ratio were taken based on the feasibility of the actual operation, and the optimal conditions were adjusted as follows: the extraction time was 4.4 h, the concentration of NaOH was 0.30 mol/L, and the liquid−solid ratio was 21 mL/g. The average yield of LSHA was 52.7%, and the relative error was 0.13% compared to the predicted value. Optimal extraction conditions of WHHA were as follows: the extraction time was 3.14 h, the NaOH concentration was 0.21 mol/L, the liquid−solid ratio was 11.93 mL/g, and the maximum yield of WHHA predicted by the model was 69.8%. Considering the feasibility of the actual operation, the liquid−solid ratio is rounded to an integer value, and the optimal conditions were adjusted as follows: extraction time was 3.1 h, NaOH concentration was 0.21 mol/L, liquid to solid ratio was 12 mL/g, and the average yield of WHHA was 69.5%, with the relative error of 0.5% compared with the predicted value. The results demonstrate that the model had good predictability, was feasible in operation, and had a practical application value. Optimal extraction conditions of LSHA were as follows: extraction time of 4.4 h, NaOH concentration of 0.30 mol/L, and liquid−solid ratio of 21 mL/g. Optimal extraction conditions of WHHA were as follows: extraction time 3.1 h, NaOH concentration 0.21 mol/L, liquid−solid ratio of 12 mL/g.

3.3. Characteristics of Two HAs. The total humic acid contents of the two weathered lignites used in this study were 30.66% and 36.10%, respectively. The proximate and ultimate analyses of coal and HA samples are listed in Table 4 and Table 5. Compared with WH, LS contains a higher moisture content. According to the classification of coal quality grades,[23,24] WH belongs to the category of extremely high ash content coal (A_d > 40%) and high volatile matter coal (37% < V_{daf} < 50%), while LS belongs to the category of extremely high ash content coal (A_d > 40%) and extremely high volatile matter coal (V_{daf} > 50%).

Table 5. Ultimate Analyses[a]

Sample	Atomic ratios				
	H/C	O/C	N/C	PI	ω
WH	0.87	0.33	0.03	-	-
LS	0.64	0.34	0.01	-	-
WHHA	0.80	0.38	0.018	0.52	0.006
LSHA	0.86	0.45	0.019	0.62	0.088

[a]PI is polarity index, calculated by (O + N)/C;[25−27] ω is the internal oxidation degree, calculated by (2O + 3N − H)/C.[18,28]

The ash yields of HAs were 4.12% and 5.09%, and the moisture contents were 8.74% and 10.64%. The results reflected that the purity of the two HAs was high. The higher organic matter content in WHHA compared to that in LSHA suggests that the former may possess a more complex molecular structure or a higher concentration of bioactive compounds, which could potentially lead to enhanced functional properties. According to elemental analysis, although the sources of the two HAs were different, the elemental compositions of the HA samples were similar (Table 4). In all samples, the elemental composition of HA has shown a range similar to those described in the literature.[1,29]

https://doi.org/10.1021/acsomega.4c01840
ACS Omega 2024, 9, 38409−38422

Table 6. Acidic Functional Groups, UV−vis, and FTIR Parameters of HAs

Sample	Total acid group content (meq/g)	Carboxyl content (meq/g)	Phenolic hydroxyl content (meq/g)	E_4/E_6	ΔLog K	Aromaticity (f_a, FTIR based)
WHHA	4.82	3.25	1.57	3.91	0.61	0.61
LSHA	5.37	3.59	1.78	4.59	0.69	0.57

The H/C and O/C atomic ratios, which are considered to be important indicators of the aromaticity and maturity of HAs, have been used to study the structural changes of humus.[30,31] The similarity in the H/C ratio between WHHA and WH coal samples indicates that they have comparable maturity levels, suggesting that WHHA has preserved the original chemical structural characteristics of WH coal samples to a good extent. The H/C ratio of LSHA is somewhat higher compared to that of the LS coal sample, which may be attributed to the possible destruction or alteration of some aromatic structures in the coal, resulting in a relative decrease in the carbon content. This phenomenon can be attributed to the difference in extraction conditions. The H/C ratios of the two types of HA were less than 1, indicating that the maturity of these two types of HAs was higher, and the maturity of weathered lignite HAs was higher than that of previously studied lignite HAs.[32] The aromaticity of the samples under study decreases with the H/C ratio. Thus, LSHA had the lowest aromatic degree (Table 5). Compared with the existing research, the aromatic degree of weathered lignite HA was higher than lignite HA.[32] The O/C atomic ratio reflects the number of oxygen-containing groups (e.g., carboxylic acids) in HAs. The O/C ratio of coal HA generally ranges from 0.32 to 0.54,[30,33] while the O/C ratios of the HAs in this paper were 0.38 and 0.45 (Table 5). The O/C ratio of LSHA was much higher than that of WHHA, which may be due to the high ash content in LSHA. The N/C atomic ratio reflects the content of nitrogen in HA. A higher N/C ratio (usually around 0.05) is characteristic of HA in soil and peat. The N/C ratio of coal HA is generally less than 0.05,[31] and the N/C ratios of the two HAs are within this range. In terms of O/C and N/C, HAs are similar to coal samples.

The polarity index ((O + N)/C) can be used to predict the adsorption behavior of HAs according to the characteristics of the organic phase.[25] The (O + N)/C values of HAs used in this work are summarized in Table 5. There is almost no difference from those reported in the literature.[25,26] The greater the value of the (O + N)/C ratio, the greater the polarity. Obviously, compared with WHHA, LSHA is more polar, indicating that the content of the polar structure is higher. The polarity order indicated by the (O + N)/C value is the same as that of the O/C value, so it is speculated that the polarity of HAs is mainly determined by oxygen-containing functional groups. Internal oxidation degree (ω) indicates the degree of the HA oxidation process. The higher its value, the higher the degree of humification. The order of the ω value was as follows: LSHA < WHHA. This outcome may indicate that LSHA experienced fewer oxidative reactions or microbial transformation processes during its formation. The ω value of weathered lignite is positive, which is the characteristic value under aerobic conditions.[34]

Acid functional groups in HA play an important role in HA application. Table 6 shows the acid functional groups of the two HAs. The contents of total acid groups and carboxyl groups of the HAs are LSHA > WHHA, while the contents of phenolic hydroxyl groups are LSHA > WHHA. The carboxyl group has a significant contribution to the solubility, buffer capacity, and cation exchange capacity of humic acid. Therefore, LSHA is more attractive in agricultural applications where nutrient retention and remediation are key issues. UV−vis spectroscopy is a nondestructive and simple method that has been used to determine the properties of HA for many years. There is a common understanding that the E_4/E_6 ratio decreases with the increase of condensed ring, humification degree, molecular weight, or size.[35] Data in Table 6 show that the E_4/E_6 ratio is lower than 6 and increases in the following order: WHHA < LSHA. Thus, it can be inferred that the molecular weight of WHHA is greater than that of LSHA. The above order is almost determined by the ΔLog K values, which confirm that the humification degree of sample WHHA is higher than that of LSHA. In addition, the ΔLog K values of the two HAs are 0.61 and 0.69, indicating that the two HAs belong to type B humic acid.

In order to better understand the findings, FTIR spectroscopy was performed to confirm the chemical structure of extracted HA from coal samples (Figure 4). The main

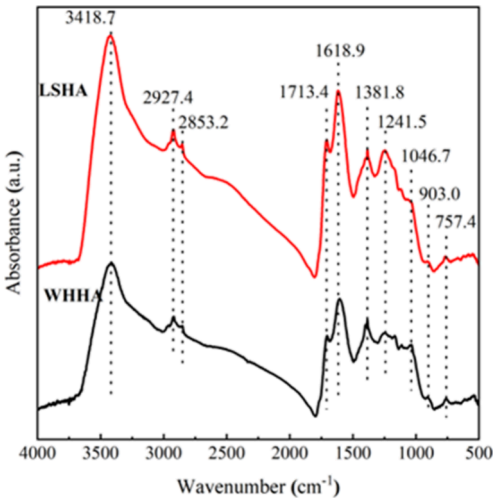

Figure 4. Fourier transform infrared spectroscopy (FTIR) spectra of LSHA and WHHA.

absorption positions of the two HAs were roughly similar, but there were significant differences in the relative intensity of certain bands among different entities, which were related to the source and nature of the samples. The valence vibration of the O−H group in the aromatic and aliphatic regions of HA appeared at 3450−3400 cm^{-1}. This confirms the hydrophilicity of HA, which is crucial for its interaction with water and other polar solvents. The broader peak of the O−H stretching vibration may be attributed to the high O/C and H/C ratios.[18] The alcoholic and amide N−H nonbonded groups showed a deep absorption band at 3418 cm^{-1}, confirming the presence of these groups.[36] The aliphatic C−H stretching in HA appeared at 2930−2850 cm^{-1}.[37] The length and branching of these chains can significantly impact the solubility, reactivity, and adsorption properties of HA. In the range of 2700−2500

https://doi.org/10.1021/acsomega.4c01840
ACS Omega 2024, 9, 38409−38422

cm^{-1}, O−H in the carboxyl group exhibited a stretching vibration.[38] A small peak appeared in the range of 1700−1720 cm^{-1} that was attributed to the stretching vibration of the C═O bond in the carboxyl group.[37] It can be seen from Figure 4 that at 1618 cm^{-1} the sharp edge loop band prominently indicates the presence of the C═ C stretch (aromatic ring). The deformation vibrations of methylene and methyl groups occurred in the spectra at 1381 cm^{-1}.[1] In the range of 1200−1260 cm^{-1}, the characteristic peaks are caused by the C−O vibration in aryl ethers and to the C−O stretching and O−H bending of carboxylic acids and/or phenolic units.[39,40] At about 1046 cm^{-1}, the C−O stretching vibration in the polysaccharide and the Si−O stretching vibration in the silicate led to the appearance of this peak, which was often attributed to the mineral matter of the sample.[1,36,41] The bands occurring in the 900−700 cm^{-1} range is assigned to the out-of-plane bending vibration of aromatic C−H bonds.[18,29] The bands observed in FTIR showed that it was evident that humic acids had an aromatic structure and contain aliphatic side chains. In addition, HA in coal samples has a complex heterogeneous chemical structure, which varies greatly with the source and properties of coal.

The range of 1500−1800 cm^{-1} contains the absorption peak for oxygen-containing functional groups (Figure 5). The area

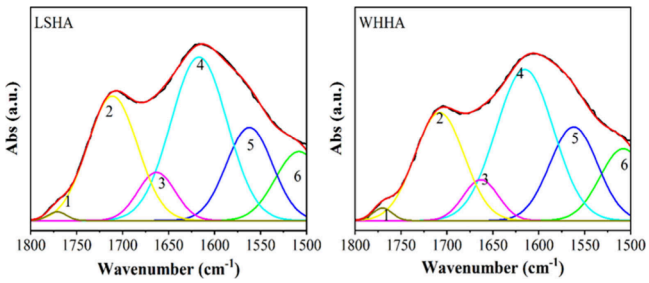

Figure 5. Oxygen functional group peaks of LSHA and WHHA

of each peak was integrated and normalized to obtain the relative percentage of each absorption peak. The results are shown in Table S3. It illustrated that the carboxyl content of the studied HAs was in the order of LSHA > WHHA, which was consistent with the determination results of acid functional groups in Table 6. The aromaticity (f_a (FTIR)) of HAs can be calculated by the corresponding peak area in the FTIR spectrum.[42] Its results are listed in Table 6 and are consistent with the elemental analysis.

The XRD patterns of LSHA and WHHA are presented in Figure 6. The amorphous nature is predominant in the two humic acids. The XRD pattern of the isolated humic acids also indicated low impurities. Broad peaks are observed at $2\theta = 25°$, indicating that HAs possess more aromatic carbon. This wide peak feature is usually associated with the complexity and amorphous properties of organic substances. The XRD approach can be used to analyze the aromatic degree of HA. It also allows for the calculation of structural parameters such as the average thickness of microcrystalline structure stacking (L_c), the spacing between carbon planes (d_{002}), the average number of carbon plane stacking layers (N), and the purity of HA.[43−46] However, there are few studies on its application to coal HA. Schweitzer et al.[43] divided the XRD patterns of HA into three zones, namely, γ band (distance between layers, 0.43 nm), G band (distance between layers, 0.35 nm), and 10 band (distance between layers, 0.23 nm). The γ band was a peak at

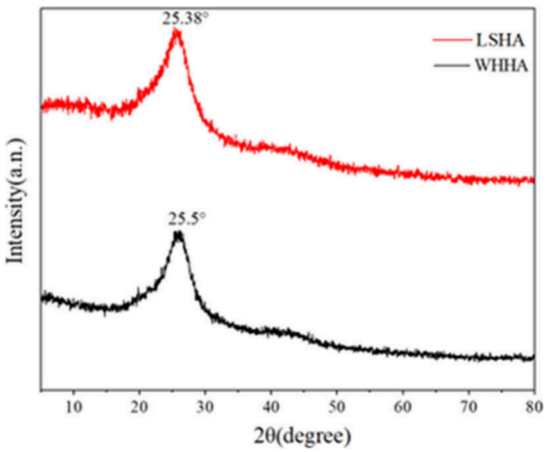

Figure 6. X-ray diffraction profiles of the studied HAs.

around $2\theta = 20°$ that was attributed primarily to aliphatic side chains, and the G (002) band was at $2\theta = 25°$, which was due to aromatic carbon.

The XRD profiles of the HAs after waveform separation are shown in Figure 7 to obtain the aroma and corresponding

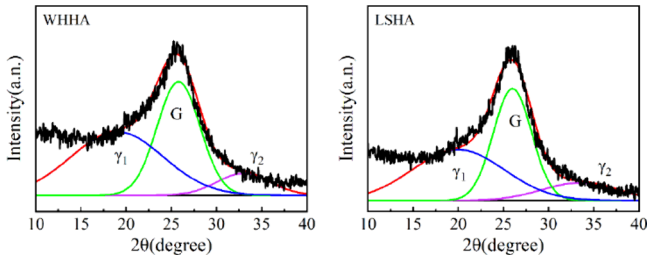

Figure 7. Fitted-peak curves of XRD patterns of four HAs.

Table 7. XRD and CP/MAS ^{13}C NMR Parameters of Four HAs

Sample	d_{002} (Å)	L_c (Å)	N	$f_{a\text{-XRD}}$	$f_{a\text{-NMR}}$	$f_{ar/al}$	$f_{h/h}$
WHHA	3.45	14.73	4.27	0.48	0.65	2.95	0.29
LSHA	3.43	16.73	4.88	0.46	0.64	3.05	0.36

parameters of HA (Table 7). The peak-fitting results are shown in Table S4. The aromatic degree of the HAs was WHHA > LSHA, which was in agreement with the FITR and elemental analysis results. The layer space d_{002} of the studied HAs was not different, at around 3.4 Å. This may mean that the interaction forces between the two HA molecules are similar. The order of stacking thickness L_c and layer number N was WHHA > LSHA, which was related to the number of aromatic structures in HA. It indicates that WHHA molecular layers are more tightly stacked in the vertical direction, and the number of stacked layers is greater. This may be due to the fact that WHHA molecules contain more aromatic ring structures, which enhances the $\pi-\pi$ interaction between molecules and promotes the stacking of molecular layers.

The CP/MAS ^{13}CNMR spectra of two kinds of HAs are shown in Figure 8. All the spectra show weak signals in the range of 240−165 ppm. These signals may arise mainly from carbonyl carbon. The small but distinct signals between 190 and 165 ppm appear to arise mainly from carboxyl carbon in

https://doi.org/10.1021/acsomega.4c01840
ACS Omega 2024, 9, 38409−38422

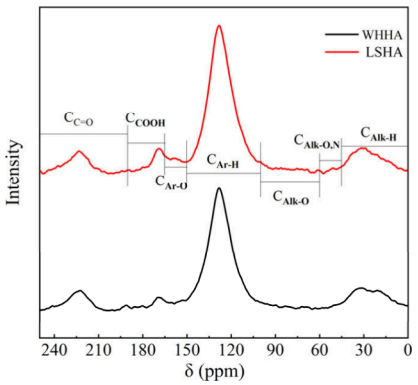

Figure 8. CP/MAS ^{13}CNMR spectra of the HAs.

HA. Strong signals appear between 165 and 100 ppm in the range corresponding approximately to the aromatic carbons. The aliphatic carbons show signals in the range of 100−0 ppm.[42] It can be seen from Figure 8 that the aromatic carbon content of the HAs is higher than that of the aliphatic carbon. Moreover, the content of aliphatic carbon in weathered lignite is lower than that in lignite.[32]

The relative content of different types of carbon atoms in HA was obtained by CP/MAS ^{13}C NMR spectroscopy and peak fitting. Figure 9 is the fitting result of the two HAs' CP/

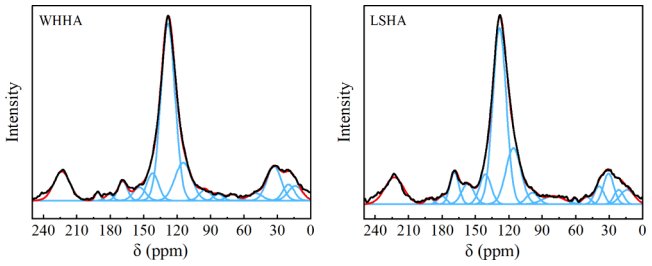

Figure 9. Peak fitting curves of CP/MAS ^{13}C NMR spectra of the two HAs.

MAS ^{13}CNMR spectra. After the classification of the functional groups containing carbon and the chemical displacement were obtained by peak separation processing on each level of the spectrogram, the relative content of each type of carbon was calculated according to the area of the fitted peak (Table S5). The relative content of aliphatic carbon (0−100 ppm) of the two HAs was WHHA (21.96%) > LSHA (20.67%). This indicates that WHHA may contain more aliphatic chains or branched chains, which may affect its solubility and biodegradability. The relative content of aromatic carbon (100−165 ppm) was WHHA (64.73%) > LSHA (63.93%), which was consistent with the XRD analysis. The relative contents of carboxyl carbon (165−190 ppm) of the two HAs were as follows: LSHA (5.97%) > WHHA (4.14%), which was consistent with the trend of carboxyl carbon content measured by the calcium acetate method in Table 6. The relative contents of the phenolic hydroxyl carbon (150−165 ppm) of the two HAs were LSHA (4.24%) > WHHA (2.91%), which was consistent with the trend of phenolic hydroxyl size analysis in Table 6. WHHA and LSHA have significant differences in structure, mainly in the contents of aromatic carbon and fatty carbon. These differences may result from differences in their original origin and subsequent weathering or treatment processes.

The related parameters in the CP/MAS^{13}CNMR of the HAs are summarized in Table 7. The degree of aromaticity ($f_{a\text{-}NMR}$) of the two HAs was WHHA > LSHA. This result was consistent with the XRD and FTIR analysis results. The hydrophilic−hydrophobic parameter ($f_{h/h}$) was LSHA > WHHA, indicating that LSHA has the most hydrophilic groups. Thus, LSHA exhibited the highest biological activity in agricultural application.[47] This may be related to the extraction conditions. The extraction time and NaOH concentration for LSHA are both higher than those for WHHA, which facilitates a more effective disruption of the coal sample structure during the extraction process, releasing more bioactive components. Additionally, factors such as the type of coal sample, the degree of weathering, and environmental conditions can all potentially influence the biological activity of humic acid.

Figure 10 shows the TG and DTG curves for the HA samples studied, and data are given in Table 8. TG curves of

Table 8. Mass Changes of the Two HAs

Sample	25−200 °C	200−350 °C	350 −600 °C	450−600 °C	Remnant
WHHA	13.57%	7.03%	75.28%	46.50%	4.12%
LSHA	11.69%	10.86%	69.93%	52.96%	5.52%

the studied samples showed gradual weight loss as a function of temperature increase. As observed, the thermal analysis of analyzed samples indicated the occurrence of three decomposition stages for LSHA and WHHA.[18]

The first one, between 28 and 180 °C, corresponded to a mass loss of 11.6 9% and 13.57%; the second one, between 200 and 350 °C, corresponded to a mass loss of 10.86% and 7.03%; and the third one, between 350 and 600 °C, corresponded to a

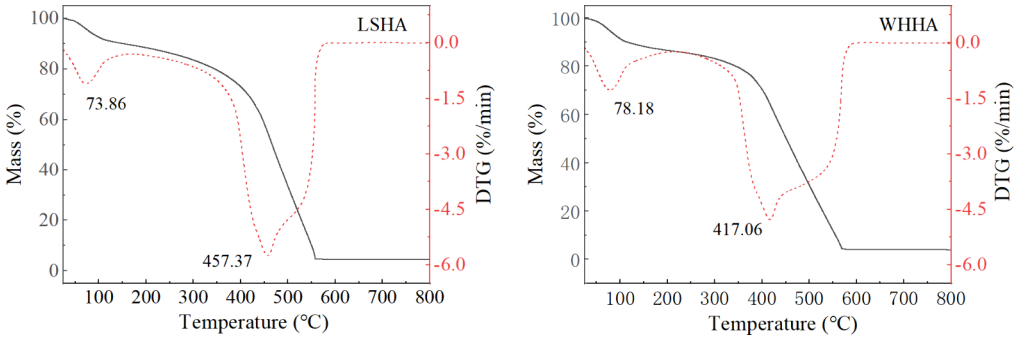

Figure 10. TG-DTG curves of the two HAs.

https://doi.org/10.1021/acsomega.4c01840
ACS Omega 2024, 9, 38409−38422

mass loss of 69.93% and 75.28%. After that, weight loss remains steady, without further observable features, until the highest temperature was measured. The residual mass at 800 °C was around 5.52% and 4.12%. The first stage was attributed to the loss of free water (dehydration) from the HA sample. The second stage was associated with the degradation of polysaccharides, the decarboxylation of acidic groups, and the dehydration of aliphatic alcohols. The third stage (which showed a larger mass loss) was attributed to the decomposition of aromatic structures and cleavage of C−C bonds.[48] Consequently, the strong exothermic peaks at approximately 457 and 417 °C showed a larger number of aromatic structures relative to the aliphatic structures in the HAs. Also, sample WHHA seems to be slightly more resistant to thermal degradation than LSHA, since the decomposition of the former samples occurs at relatively higher temperatures.[49] This indicates that the aromatic structure in WHHA samples may be more complex or more cross-linked, thereby improving its thermal stability. In the total analyzed temperature range the weight loss was higher for WHHA than for LSHA, which could be connected with the lower humification degree (the lower values of N/C).[50] The differences exhibited by WHHA and LSHA samples during TGA may result from a combination of factors, such as their original sources, extraction methods, environmental conditions, and subsequent processing procedures. Together these factors determine the HA's chemical composition, structure, and properties of the sample.

XPS has been used to characterize the surface elemental compositions of LSHA and WHHA.[1] As Figure 11 displays,

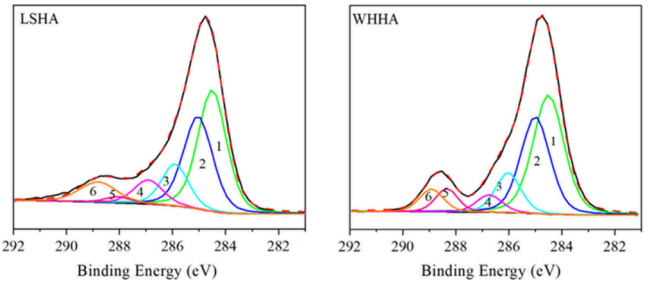

Figure 11. Fitted-peak curves of C 1s spectra of the two HAs.

the XPS C 1s spectrum of HAs was fitted with 6 peaks at 284.4 ± 0.2, 285.0 ± 0.2, 286.0 ± 0.2, 286.8 ± 0.2, 288.1 ± 0.2, and 288.8 ± 0.2 eV, corresponding to aromatic, aliphatic, ether/alcohol, ketonic, pyrrole/amide, and carboxyl carbons, respectively. The chemical assignments, binding energy (BE), and relative proportion (RP) of each functional group in the C 1s spectra of HA fractions are listed in Table 9. Aromatic carbon and aliphatic carbon were the main forms of carbon element present on the surface of the HAs, which was consistent with ^{13}C NMR data. In addition, the relative proportion of carboxylic carbon in LSHA (8.50%) was higher than that of WHHA (6.06%), which indicates that LSHA contains more carboxyl than WHHA. These results are in line with data from the FTIR and acid functional groups and CP/MAS ^{13}CNMR of the HAs. For the XPS O 1s signals, four peaks were fitted as shown in Figure 12. Chemical assignments and binding energy values of the peaks were C═O (531.7 ± 0.2 eV), C−O (532.7 ± 0.2 eV), COO (533.5 ± 0.2 eV), and adsorbed oxygen (534.6 ± 0.2 eV), respectively.[51] The experimental area percentages for each component of the O 1s spectra of HAs are listed in Table 10. The data demonstrated that the main form of surface oxygen elements of the HAs was C═O, followed by C−O and COO, and the adsorbed oxygen content of the two samples was low. The above results show that the HAs from weathered lignite and previously studied HAs from lignite[32] have a very similar chemical composition.

The fluorescence index (FI) is a parameter used to distinguish organic matter derived from terrestrial and microbial sources. It is the ratio of the fluorescence intensity at 450/500 nm in the emission spectrum (with a fixed excitation wavelength of 370 nm). According to Table 11, the FI values of the HAs were 1.15−1.36, indicating that the two HAs belonged to terrestrial HAs.[1] The biological index (BIX) values of the two HAs were less than 1, indicating that the content of primary organic matter of the two HAs was less, which was consistent with the results in the literature,[1] and the content of primary organic matter of weathered lignite HA was less than that of lignite HA. This may be due to the fact that microbial activity and chemical decomposition during weathering further reduce the content of primary biomass.

The fluorescence excitation spectra of the studied HAs are shown in Figure 13(a). The excitation spectra of LSHA and WHHA featured one intense peak at about 270 nm. This peak position is usually associated with the aromatic structure or conjugate system in the HA molecule, indicating that both LSHA and WHHA contain a certain number of aromatic compounds. The fluorescence emission spectra of LSHA and WHHA are shown in Figure 13(b). The values of the fluorescence intensity (in arbitrary units, au) and fluorescence maxima are presented in Table 11. The intensity of WHHA was significantly higher than LSHA, which was attributed to the fact that WHHA had more aromatic structures replaced by electron-donating groups or more aromatic structures were replaced by electron-withdrawing groups and/or an unsaturated conjugate structure because the HA molecules of electron-withdrawing groups (for example, carboxyl and carbonyl) can make the fluorescence intensity of HA decrease and electronic groups (such as amino, hydroxyl, methods, etc.) can make the fluorescence intensity of HA increase. The presence of these oxygen-containing and nitrogen-containing functional groups can transfer fluorescence to longer wavelengths by reducing the energy difference between the ground state and the first excited state.[36,52,53]

The impact of scattered light on the spectrum and spectral overlap can be reduced by using a synchronous fluorescence

Table 9. Fitted-Peak Results of C 1s Spectra of the Two HAs[a]

	Aromatic		Aliphatic		Ether/Alcohol		Ketonic		Pyrrole		Carboxylic	
Sample	BE	RP	BE	RP	BE	RP	BE	RP	BE	RP	BE	RP
WHHA	284.48	40.76	285.07	31.31	286.10	11.20	286.77	4.93	288.24	5.74	288.87	6.06
LSHA	284.50	38.77	285.04	30.44	285.90	12.52	286.90	7.95	288.06	1.82	288.81	8.50

[a]BE is binding energy, eV; RP is relative percentage, %.

https://doi.org/10.1021/acsomega.4c01840
ACS Omega 2024, 9, 38409−38422

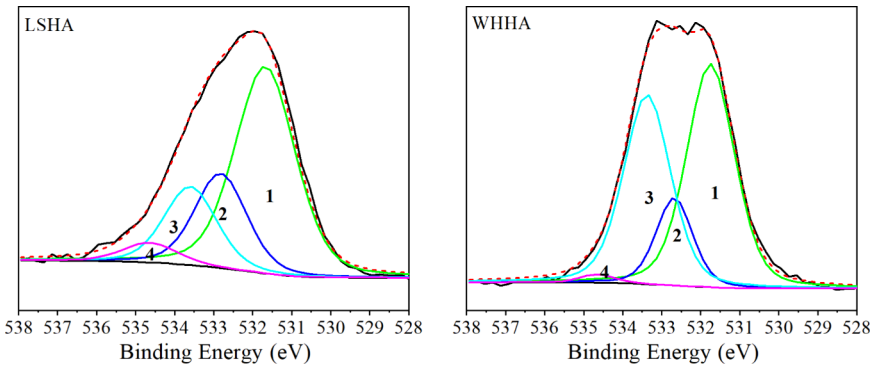

Figure 12. Fitted-peak curves of O 1s spectra of HAs.

Table 10. Fitted-Peak Results of O 1s Spectra of HAs[a]

	LSHA		WHHA	
Sample	BE	RP	BE	RP
C═O	531.68	55.32	531.74	46.25
C−O	532.82	21.65	532.67	13.86
COO	533.59	18.20	533.38	38.64
Adsorbed oxygen	534.64	4.82	534.66	1.25

[a]BE is binding energy, eV; RP is relative percentage, %.

Table 11. Fluorescence Parameters and Maximum Emission Wavelength of HAs

			E_m	
Sample	FI	BIX	λ_{max} (nm)	I (au)
WHHA	1.36	0.49	414.2	130.6
LSHA	1.15	0.39	437.0	125.2

spectrum. The most commonly used step length $\Delta\lambda$ (difference between the emission wavelength and excitation wavelength) is 18 nm.[53] The synchronous fluorescence spectra of the HAs are shown in Figure 13(c). As can be observed, there were three obvious peaks in the synchronous fluorescence spectra of LSHA and WHHA, indicating that LSHA and WHHA had more complex structures and stronger dispersion. It may arise from the presence of different functional groups and structures in HA molecules, which contribute differently to fluorescence emission. In contrast, the previously studied lignite had the simplest structure and the least dispersion, which reflects the relatively unitary composition of its molecules.[32,53] This reflects the relative uniformity of its molecular composition. In addition, when the excitation wavelength E_x of synchronous fluorescence spectrum ($\Delta\lambda$ = 18 nm) is in the range of 340−370 nm, the corresponding polycyclic aromatic hydrocarbons (PAHs) are composed of 3−4 viscous benzene rings; when E_x is in the range of 370−420

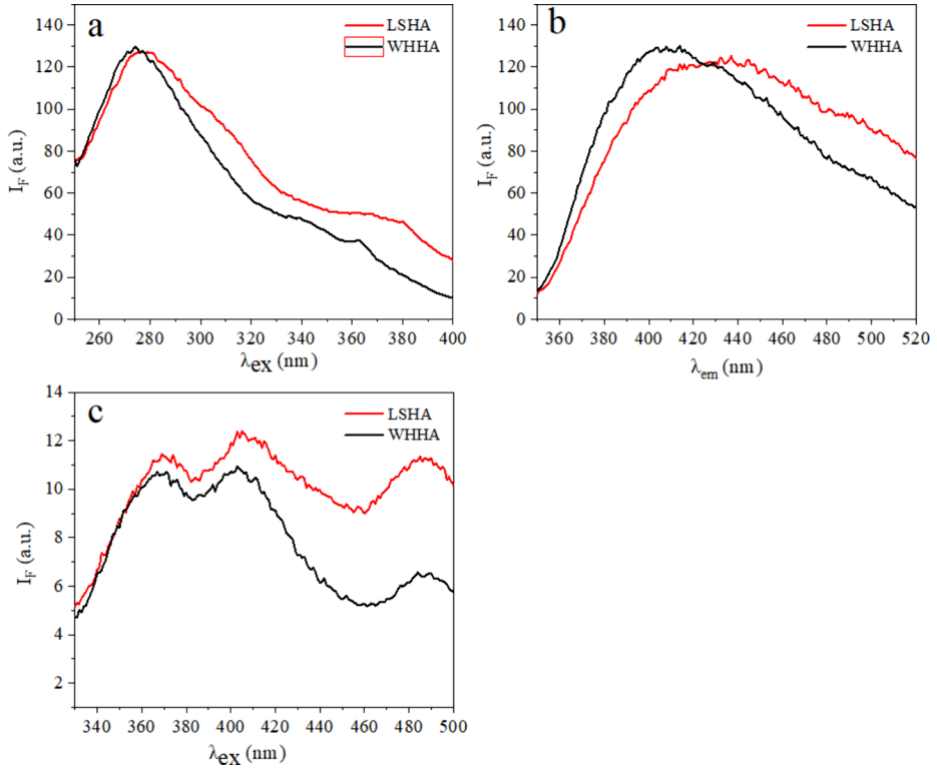

Figure 13. Excitation spectra (a), emission spectra (b), and synchronous fluorescence (c) of the two HAs ($\Delta\lambda$ = 18 nm).

https://doi.org/10.1021/acsomega.4c01840
ACS Omega 2024, 9, 38409−38422

Table 12. Location and Intensity of Ex/Em Peaks of HAs

	Peak 1		Peak 2		Peak 3	
Sample	Ex/Em	I	Ex/Em	I	Ex/Em	I
YLHA	270/450	31.24	280/310	20.17	340/440	21.47
HBHA	260/450	39.98	270/420	39.81	280/310	24.39
WHHA	270/410	122.10	280/310	16.51	-	-
LSHA	270/440	113.80	280/310	17.22	280/450	113.90

nm, the corresponding PAHs are composed of 5 benzene rings; and when E_x is in the range of 438−487 nm, the corresponding PAHs have about 7 benzene rings or molecules containing lignin structures.[54] Therefore, the PAHs in LSHA and WHHA were composed of three to five thickened benzene rings and were mainly composed of five thickened benzene rings. The HAs also contained a small amount of PAHs consisting of about seven fused benzene rings and lignin structures.

Table 12 shows that the EEM wavelength range is consistent with that in the literature, indicating that the two HAs both belong to coal HA,[1] and that the Ex/Em peak positions of the two HAs are very similar, indicating that the fluorophore in the two HA samples is the same or similar. The similarity of fluorophore may mean the two HA have common characteristics in structure and functional groups. When the excitation wavelength is 245−280 nm and the fluorescence emission wavelength is 340−400 nm, PAHs are composed of three condensed benzene rings. When the emission wavelength is 400−450 nm, PAHs are composed of four aromatic rings. When the λ_{em} > 450 nm, PAHs may be composed of more than four benzene rings.[1,55] As displayed in Table 12, PAHs composed of four thickened benzene rings exist in the two raw coal HAs. The results were in good agreement with those obtained by fluorescence synchronous spectroscopy.

4. CONCLUSIONS

In this study, response surface methodology was employed to develop an efficient model aimed at optimizing the extraction of humic acids from two types of weathered lignite. The RSM outcomes for LSHA (R^2 = 0.9752) and WHHA (R^2 = 0.9892) indicated a high fitness of the models for predicting HA extraction efficiency. The extraction efficiency of HAs is governed by a confluence of factors, encompassing extraction time, NaOH concentration, the liquid-to-solid ratio, and their interactive effects. Additionally, regional differences emerged as a pivotal consideration that cannot be overlooked. The optimal extraction conditions were identified as 4.4 h for extraction time, 0.30 mol/L NaOH concentration, and a liquid-to-solid ratio of 21 mL/g for LSHA, whereas for WHHA, these were 3.1 h, 0.21 mol/L NaOH, and a ratio of 12 mL/g. The actual and predicted yields fell within the acceptable relative error limits.

UV−vis, FTIR, XPS, and fluorescence spectroscopy confirmed the presence of carboxyl, phenolic, ketonic, aromatic, and aliphatic functional groups in HAs extracted from weathered lignite. Notably, WHHA exhibited a higher aromaticity than LSHA, suggesting potentially greater chemical reactivity and adsorption capacity. The high aromatic carbon content and low aliphatic carbon content in WHHA likely contribute to its enhanced structural stability and reduced biodegradability. However, the abundant carboxyl and phenolic carbon in LSHA may confer heightened environmental reactivity and biological activity. This finding was further corroborated by hydrophilic−hydrophobic parameters. WHHA samples demonstrated superior thermal stability compared to LSHA. Both belonged to terrestrial HAs with a relatively low native organic matter content. The polycyclic aromatic hydrocarbons in LSHA and WHHA were predominantly composed of three to five benzene rings, with trace amounts of higher-ring PAHs.

The subtle differences in chemical composition and structure between LSHA and WHHA can be traced back to their original coal samples, weathering degrees, and subsequent processing procedures. Weathering processes alter the chemical composition and structure of coal samples, thereby influencing the properties of the extracted HAs. Furthermore, variations in treatment conditions may lead to changes in the distribution and content of functional groups within the HAs. Environmental pollution and resource waste can be reduced by optimizing the extraction process. In the future, the RSM can be extended to predict the extraction efficiency of different coal sources with different properties. The results of this study provide strong support for the sustainable utilization of HA.

■ ASSOCIATED CONTENT

Supporting Information

The Supporting Information is available free of charge at https://pubs.acs.org/doi/10.1021/acsomega.4c01840.

Effects of single factors on the yield of HAs; factors and levels of BBD-RSM design; fitted-peak assignment of FTIR; fitted-peak results of XRD; and fitted-peak results of CP/MAS ^{13}C NMR (PDF)

■ AUTHOR INFORMATION

Corresponding Author

Yanhong Li − *Faculty of Chemical Engineering, Kunming University of Science and Technology, Kunming 650500, People's Republic of China;* orcid.org/0000-0001-6434-2761; Email: liyh_2004@163.com

Authors

Yan Yang − *Faculty of Chemical Engineering, Kunming University of Science and Technology, Kunming 650500, People's Republic of China;* orcid.org/0009-0004-3877-3399

Yuanqin Zhang − *Faculty of Chemical Engineering, Kunming University of Science and Technology, Kunming 650500, People's Republic of China*

Miao Wang − *Faculty of Chemical Engineering, Kunming University of Science and Technology, Kunming 650500, People's Republic of China*

Pingyan Wang − *Faculty of Chemical Engineering, Kunming University of Science and Technology, Kunming 650500, People's Republic of China*

https://doi.org/10.1021/acsomega.4c01840
ACS Omega 2024, 9, 38409−38422

Donghui Liu − *Faculty of Chemical Engineering, Kunming University of Science and Technology, Kunming 650500, People's Republic of China*

Complete contact information is available at: https://pubs.acs.org/10.1021/acsomega.4c01840

Notes

The authors declare no competing financial interest.

■ ACKNOWLEDGMENTS

The authors thank the financial support provided by the National Natural Science Foundation of China (21766013) and Analysis and Testing Foundation of Kunming University of Science and Technology (2020M20192208013).

■ REFERENCES

(1) Doskočil, L.; Burdíková-Szewieczková, J.; Enev, V.; Kalina, L.; Wasserbauer, J. Spectral characterization and comparison of humic acids isolated from some European lignites. *Fuel* **2018**, *213*, 123−132.
(2) de Melo, B. A.; Motta, F. L.; Santana, M. H. Humic acids: Structural properties and multiple functionalities for novel technological developments. *Mater. Sci. Eng. C Mater. Biol. Appl.* **2016**, *62*, 967−74.
(3) Havelcova, M.; Mizera, J.; Sykorova, I.; Pekar, M. Sorption of metal ions on lignite and the derived humic substances. *J. Hazard Mater.* **2009**, *161* (1), 559−64.
(4) Nardi, S.; Pizzeghello, D.; Muscolo, A.; Vianello, A. Physiological effects of humic substances on higher plants. *J. Soil Biology Biochemistry***2002**, *34* (11), 1527.
(5) Sun, Z.; Tang, B.; Xie, H. Treatment of Waste Gases by Humic Acid. *Energy Fuels* **2015**, *29* (3), 1269−1278.
(6) Peña-Méndez, E. M., H, J., Patočka, J., Humic substances-compounds of still unknown structure: applications in agriculture, industry, environment, and biomedicine. *Journal of Applied Biomedicine* **2005**, *3*, 13.
(7) Dong, L. H.; Yang, J. S.; Yuan, H. L.; Wang, E. T.; Chen, W. X. Chemical characteristics and influences of two fractions of Chinese lignite humic acids on urease. *European Journal of Soil Biology* **2008**, *44* (2), 166−171.
(8) Qian, S.; Ding, W.; Li, Y.; Liu, G.; Sun, J.; Ding, Q. Characterization of humic acids derived from Leonardite using a solid-state NMR spectroscopy and effects of humic acids on growth and nutrient uptake of snap bean. *Chemical Speciation & Bioavailability* **2015**, *27* (4), 156−161.
(9) Trinh, T. K.; Kang, L. S. Response surface methodological approach to optimize the coagulation−flocculation process in drinking water treatment. *Chem. Eng. Res. Des.* **2011**, *89* (7), 1126−1135.
(10) Betiku, E.; Omilakin, O. R.; Ajala, S. O.; Okeleye, A. A.; Taiwo, A. E.; Solomon, B. O. Mathematical modeling and process parameters optimization studies by artificial neural network and response surface methodology: A case of non-edible neem (Azadirachta indica) seed oil biodiesel synthesis. *Energy* **2014**, *72*, 266−273.
(11) Sarlaki, E.; Sharif Paghaleh, A.; Kianmehr, M. H.; Asefpour Vakilian, K. Valorization of lignite wastes into humic acids: Process optimization, energy efficiency and structural features analysis. *Renewable Energy* **2021**, *163*, 105−122.
(12) Wang, C.-F.; Fan, X.; Zhang, F.; Wang, S.-Z.; Zhao, Y.-P.; Zhao, X.-Y.; Zhao, W.; Zhu, T.-G.; Lu, J.-L.; Wei, X.-Y. Characterization of humic acids extracted from a lignite and interpretation for the mass spectra. *RSC Adv.* **2017**, *7* (33), 20677−20684.
(13) Haider, R.; Ghauri, M. A.; Akhtar, K. Isolation of Coal Degrading Fungus from Drilled Core Coal Sample and Effect of Prior Fungal Pretreatment on Chemical Attributes of Extracted Humic Acid. *Geomicrobiology Journal* **2015**, *32* (10), 944−953.
(14) Jia, J.; Zhang, Y.; Liu, Q.; Huang, G.; Xing, B.; Zhang, C.; Guo, H.; Pan, J.; Cao, Y. Characterization of coal-based humic acids in relation to their preparation methods. *Energy Sources, Part A: Recovery, Utilization, and Environmental Effects* **2020**, 1−11.
(15) Li, S. *Humic Acid Product Analysis and Standards*; Chemical Industry Press, 2007.
(16) GB/T212−2008, Proximate Analysis of Coal. *National Standard of the People's Republic of China*; 2008.
(17) Klavins, M.; Purmalis, O. Properties and structure of raised bog peat humic acids. *J. Mol. Struct.* **2013**, *1050*, 103−113.
(18) Das, T.; Saikia, B. K.; Baruah, B. P.; Das, D. Characterizations of humic acid isolated from coals of two Nagaland Coalfields of India in relation to their origin. *Journal of the Geological Society of India* **2015**, *86*, 468−474.
(19) Cheng, G.; Niu, Z.; Zhang, C.; Zhang, X.; Li, X. Extraction of Humic Acid from Lignite by KOH-Hydrothermal Method. *Applied Sciences* **2019**, *9* (7), 1356.
(20) Li, Y.; Yuan, S. Influence of addition of KOH on the yield and characteristics of humic acids extracted from lignite using NaOH. *SN Applied Sciences* **2021**, *3* (1), DOI: 10.1007/s42452-020-04087-x.
(21) Rashid, T.; Sher, F.; Jusoh, M.; Joya, T. A.; Zhang, S.; Rasheed, T.; Lima, E. C. Parametric optimization and structural feature analysis of humic acid extraction from lignite. *Environ. Res.* **2023**, *220*, No. 115160.
(22) Tian, D. Z. W. Z. S. C. J. Optimization of Stir-fried with Salt-water Technology in Plantain Seed by BBD-RSM. *Medicinal Plant* **2014**, *5* (03), 9−13.
(23) MT/T 849-2000, Classification of volatile matter yield of coal. *Coal Industry Standard of the People's Republic of China*, 2000.
(24) GB/T15224.1-2018, Classification for quality of coal-Part 1: Ash. *National Standard of the People's Republic of China*, 2018.
(25) Xing, B.; McGill, W. B.; Dudas, M. J. Cross-correlation of polarity curves to predict partition coefficients of nonionic organic contaminants. *Environ. Sci. Technol.* **1994**, *28* (11), 1929−33.
(26) Ojwang, L. M.; Cook, R. L. Environmental conditions that influence the ability of humic acids to induce permeability in model biomembranes. *Environ. Sci. Technol.* **2013**, *47* (15), 8280−7.
(27) Sun, H.; Zhu, D.; Mao, J. Sorption of polar and nonpolar aromatic compounds to two humic acids with varied structural heterogeneity. *Environ. Toxicol. Chem.* **2008**, *27* (12), 2449−56.
(28) Bożena Debska, M. D., Tobiasova, E. *Effect of Post-Harvest Residue of Maize, Rapeseed, and Sunflower on Humic Acids Properties in Various Soils*, 2012.
(29) Ibarra, J.; Juan, R. Structural changes in humic acids during the coalification process. *Fuel* **1985**, *64*, 650−656.
(30) Francioso, O.; Montecchio, D.; Gioacchini, P.; Ciavatta, C. Thermal analysis (TG−DTA) and isotopic characterization (13C−15N) of humic acids from different origins. *Appl. Geochem.* **2005**, *20* (3), 537−544.
(31) Allard, B. A comparative study on the chemical composition of humic acids from forest soil, agricultural soil and lignite deposit. *Geoderma* **2006**, *130* (1−2), 77−96.
(32) Wang, M.; Li, Y.; Zhang, Y.; Hu, X.; Li, Q.; Su, Y.; Zhao, W. Exploration of the H_2O_2 Oxidation Process and Characteristic Evaluation of Humic Acids from Two Typical Lignites. *ACS Omega* **2021**, *6* (37), 24051−24061.
(33) Nasir, S.; Sarfaraz, T. B.; Verheyen, T. V.; Chaffee, A. L. Structural elucidation of humic acids extracted from Pakistani lignite using spectroscopic and thermal degradative techniques. *Fuel Process. Technol.* **2011**, *92* (5), 983−991.
(34) Cieslewicz, J.; Gonet, S. S. Properties of humic acids as biomarkers of lake catchment management. *Aquatic. Sci.* **2004**, *66* (2), 178−184.
(35) Zalba, P.; Amiotti, N. M.; Galantini, J. A.; Pistola, S. Soil Humic and Fulvic Acids from Different Land-Use Systems Evaluated By E4/E6 Ratios. *Communications in soil science and plant analysis* **2016**, *47* (13−14), 1675−1679.
(36) Enev, V.; Pospíšilová, L.; Klučáková, M.; Liptaj, T.; Doskočil, L. Spectral characterization of selected humic substances. *Soil and Water Research* **2014**, *9* (1), 9−17.

(37) Zykova, M. V.; Brazovsky, K. S.; Veretennikova, E. E.; Danilets, M. G.; Logvinova, L. A.; Romanenko, S. V.; Trofimova, E. S.; Ligacheva, A. A.; Bratishko, K. A.; Yusubov, M. S.; Lyapkov, A. A.; Belousov, M. V. New artificial network model to estimate biological activity of peat humic acids. *Environ. Res.* **2020**, *191*, No. 109999.
(38) Baigorri, R.; Fuentes, M.; Gonzalez-Gaitano, G.; Garcia-Mina, J. M.; Almendros, G.; Gonzalez-Vila, F. J. Complementary multi-analytical approach to study the distinctive structural features of the main humic fractions in solution: gray humic acid, brown humic acid, and fulvic acid. *J. Journal of agricultural and food chemistry* **2009**, *57* (8), 3266.
(39) Novák, F.; Šestauberová, M.; Hrabal, R. Structural features of lignohumic acids. *J. Mol. Struct.* **2015**, *1093*, 179−185.
(40) Dick, D. P.; Mangrich, A. S.; Menezes, S. M. C.; Pereira, B. F. Chemical and Spectroscopical Characterization of Humic Acids from two South Brazilian Coals of Different Ranks. *J. Braz. Chem. Soc.*. **2002**, *13* (2), 177.
(41) Liebezeit, U. F. G. *An IR study of humic acids isolated from sediments and soils*, 2003.
(42) Gong, G.-q.; Zhao, Y.-f.; Zhang, Y.-j.; Deng, B.; Liu, W.-x.; Wang, M.; Yuan, X.; Xu, L.-w. Establishment of a molecular structure model for classified products of coal-based fulvic acid. *Fuel* **2020**, *267*, No. 117210.
(43) Schnitzer, M.; Kodama, H.; Ripmeester, J. A. Determination of the Aromaticity of Humic Substances by X-Ray Diffraction Analysis. *J. Soil Science Society of America Journal* **1991**, *55* (3), 745.
(44) Katsumi, N.; Yonebayashi, K.; Okazaki, M. Evaluation of stacking nanostructure in soil humic acids by analysis of the 002 band of their X-ray diffraction profiles. *Soil Science and Plant Nutrition* **2015**, *61* (4), 603−612.
(45) Ikeya, K.; Hikage, T.; Arai, S.; Watanabe, A. Size distribution of condensed aromatic rings in various soil humic acids. *Org. Geochem.* **2011**, *42* (1), 55−61.
(46) Naidja, A.; Huang, P. M.; Anderson, D. W.; Kessel, C. V. Fourier Transform Infrared, UV-Visible, and X-Ray Diffraction Analyses of Organic Matter in Humin, Humic Acid, and Fulvic Acid Fractions in Soil Exposed to Elevated CO2 and N Fertilization. *J. Appl. Spectrosc.* **2002**, *56* (3), 318.
(47) Zherebtsov, S. I.; Malyshenko, N. V.; Votolin, K. S.; Androkhanov, V. A.; Sokolov, D. A.; Dugarjav, J.; Ismagilov, Z. R. Structural-Group Composition and Biological Activity of Humic Acids Obtained from Brown Coals of Russia and Mongolia. *Solid Fuel Chemistry* **2019**, *53* (3), 145−151.
(48) Jl, M.; Dm, X.; Vs, S.; Rp, S.; Mf, M.; Sn, C.; Vn, F.; Bs, C. Characterization of the Coal Humic Acids from the Candiota Coalfield, Brazil. *International Journal of Agriculture Sciences* **2012**, *4* (5), 238−242.
(49) Giovanela, M.; Crespo, J. S.; Antunes, M.; Adamatti, D. S.; Fernandes, A. N.; Barison, A.; da Silva, C. W. P.; Guégan, R.; Motelica-Heino, M.; Sierra, M. M. D. Chemical and spectroscopic characterization of humic acids extracted from the bottom sediments of a Brazilian subtropical microbasin. *J. Mol. Struct.* **2010**, *981* (1−3), 111−119.
(50) Boguta, P.; Sokołowska, Z.; Skic, K., Use of thermal analysis coupled with differential scanning calorimetry, quadrupole mass spectrometry and infrared spectroscopy (TG-DSC-QMS-FTIR) to monitor chemical properties and thermal stability of fulvic and humic acids. *J. PLoS ONE* **2017**, *12* (12), e0189653.
(51) Li, Z.-K.; Wei, X.-Y.; Yan, H.-L.; Zong, Z.-M. Insight into the structural features of Zhaotong lignite using multiple techniques. *Fuel* **2015**, *153*, 176−182.
(52) Fuentes, M.; González-Gaitano, G.; García-Mina, J. M. The usefulness of UV−visible and fluorescence spectroscopies to study the chemical nature of humic substances from soils and composts. *Org. Geochem.* **2006**, *37* (12), 1949−1959.
(53) Rodríguez, F.; Schlenger, P.; García-Valverde, M. A comprehensive structural evaluation of humic substances using several fluorescence techniques before and after ozonation. *Part I: Structural characterization of humic substances.* **2016**, *476*−*477*, 718.
(54) Peuravuori, J.; Koivikko, R.; Pihlaja, K. Characterization, differentiation and classification of aquatic humic matter separated with different sorbents: synchronous scanning fluorescence spectroscopy *J. Water Research* **2002**, *36* (18), 4552.
(55) Doskočil, L.; Enev, V.; Pekař, M.; Wasserbauer, J. The spectrometric characterization of lipids extracted from lignite samples from various coal basins. *Org. Geochem.* **2016**, *95*, 34−40.

https://doi.org/10.1021/acsomega.4c01840
ACS Omega 2024, 9, 38409−38422